Dalton Transactions

ROYAL SOCIETY OF CHEMISTRY

PAPER

Check for updates

Cite this: *Dalton Trans.*, 2022, **51**, 17203

Elucidating the mechanism of photochemical CO_2 reduction to CO using a cyanide-bridged di-manganese complex†

Kailyn Y. Cohen, Adam Reinhold, Rebecca Evans, Tia S. Lee, Hsin-Ya Kuo, Delaan G. Nedd, Gregory D. Scholes and Andrew B. Bocarsly *

Received 1st August 2022,
Accepted 24th October 2022

DOI: 10.1039/d2dt02506j

rsc.li/dalton

The complex, $[\{[Mn(bpy)(CO)_3]_2\}(\mu\text{-}CN)]^+$ (**Mn_2CN^+**), has previously been shown to photochemically reduce CO_2 to CO. The detailed mechanism behind its reactivity was not elucidated. Herein, the photoevolution of this reaction is studied in acetonitrile (MeCN) using IR and UV-vis spectroscopy. Samples were excited into the $Mn^I \rightarrow \pi^*$ bpy metal-to-ligand charge transfer (MLCT) absorption band triggering CO loss, and rapid MeCN solvent ligation at the open coordination site. It is concluded that this process occurs selectively at the Mn axial ligation site that is *trans* to the C-end of the bridging cyanide. Upon further photolysis, the metal–metal bonded dimeric species, $[(CO)_3(bpy)Mn\text{–}Mn(bpy)(CO)_3]$ (**Mn–Mn**) is observed to form under anaerobic conditions. The presence of this dimeric species coincides with the observation of CO production. When oxygen is present, CO_2 photoreduction does not occur, which is attributed to the inability of **Mn_2CN^+** to convert to the metal–metal bonded dimer. Photolysis experiments, where the **Mn–Mn** dimer is formed photochemically under argon first and then exposed to CO_2, reveal that it is the radical species, $[Mn(bpy)(CO)_3^{\bullet}]$ (**$Mn^{\bullet}$**), that interacts with the CO_2. Since the presence of **Mn–Mn** and light is required for CO production, $[Mn(bpy)(CO)_3^{\bullet}]$ is proposed to be a photochemical reagent for the transformation of CO_2 to CO.

Introduction

Finding ways to harness solar energy to form chemical bonds *via* CO_2 reduction is desirable because they provide a promising way to recycle carbon sources by creating organic feedstocks and fuels.[1,2] To this end, complexes containing the rhenium polypyridine motif have demonstrated versatility as catalysts in electro- and photocatalytic CO_2 reduction.[3–7] There is an interest in the use of $[Mn^I(diimine)(CO)_3(X)]$ as molecular catalysts for electrocatalytic CO_2 reduction, owing to the higher natural abundance and availability of Mn as compared to Re.[2,8] In contrast to significant progress using Mn complexes for electrochemical CO_2 reduction, relatively less attention has been given to photochemical CO_2 reduction.[9,10] Certainly, this photochemical activation involves multiple electron transfer processes that may couple with protons to generate critical intermediates.[11] Therefore, thorough investigation and mechanistic insights are important in order to develop this photochemical system.

The photochemistry and photophysics of first- and third-row transition carbonyl complexes are quite different due to the important role of spin–orbital coupling in the heavy transition metals. $[Re(bpy)(CO)_3Cl]$ and related complexes, for example, emit in room temperature solution upon excitation of the MLCT states, while the manganese analog does not.[6,12] The photostability of the Re complexes under excitation of the low-lying MLCT state plays a vital role in accounting for their photocatalytic versatility.[13] In contrast, the Mn diimine tricarbonyl complexes are photolabile and undergo photochemical reaction strikingly different from those of Re complexes.[14] In the Mn complexes, excitation of the MLCT state leads to dissociation of an axial ligand as the reactive ligand field state becomes thermally populated, due to the internal conversion from the low-lying MLCT state.[14]

$[Mn(bpy)(CO)_3Br]$ has been of interest as an electrocatalyst for the reduction of CO_2 to CO since 2011.[15] However, the deleterious photochemical instability of this complex in solution under normal room light, as noted by a number of research groups, has made study of this electrochemistry challenging.[14,16–21] We now report that the observed apparent chemical instability in this class of complexes is also due to the extreme oxygen sensitivity of the photochemical intermediates. Further, we associate this oxygen sensitivity with the

Department of Chemistry, Frick Laboratory, Princeton University, Princeton, New Jersey, USA. E-mail: bocarsly@princeton.edu

†Electronic supplementary information (ESI) available. See DOI: https://doi.org/10.1039/d2dt02506j

inability of the starting material to photochemically form [(CO)$_3$(bpy)Mn–Mn(bpy)(CO)$_3$] (**Mn–Mn**), and the associated radical species, [Mn(bpy)(CO)$_3^{\bullet}$]. In coming to this conclusion, we suggest that **Mn$^{\bullet}$** is the primary species associated with the photochemical conversion of CO_2 to CO.

The results and conclusions presented here are based on photochemical studies of [(CO)$_3$(bpy)Mn^{I}–CN–Mn^{I}(bpy)(CO)$_3$]$^+$, formed by reacting [Mn(bpy)(CO)$_3$Br] with [Mn(bpy)(CO)$_3$CN] in the presence of silver perchlorate (Fig. 1).[22]

Here, we describe a mechanistic scheme based on photophysical and spectroscopic evidence for the reactivity of **Mn$_2$CN$^+$**, leading to the two-electron reduction of CO_2 to CO, along with an understanding of the unanticipated role of trace O_2 in this chemistry. Though based on the specific starting material **Mn$_2$CN$^+$**, we suggest that the reaction scheme developed here is broadly applicable to the chemistry of this class of manganese carbonyl complexes.

Results & discussion

Owing to the different binding properties of the two ends of the cyanide bridging ligand in **Mn$_2$CN$^+$** (*i.e.* pure σ-donor on the N-terminal *versus* π-acceptor on the C-end), we anticipated inequivalent metal–ligand bond strengths for the two CO ligands *trans* to the bridging cyanide ligand. This hypothesis was experimentally substantiated by the bond length difference observed between the two axial Mn–CO bonds in the crystal structure of **Mn$_2$CN$^+$**, and the two carbon signals associated with the axial carbonyl groups in the ^{13}C NMR of this complex, as reported previously and reviewed in Table 1.[22]

Based on these observations, we hypothesize that upon MLCT excitation in acetonitrile, dissociation of the axial CO *trans* to the C-end of the cyanide bridge occurs. Acetonitrile is then expected to ligate to this coordination site forming the intermediate (**s-Mn$_2$CN$^+$**) shown in Fig. 2. This specific species is hypothesized over ligand loss *trans* to the N-terminus (**Mn$_2$CN$^+$-s**) based upon the IR spectrum before and after irradiation into the MLCT band.[22]

Dissociation of a CO ligand triggered by MLCT excitation has been established in α-diimine substituted monomeric Mn complexes.[14,23–25] The photochemistry of *fac*-[Mn(bpy)(CO)$_3$X] (X = halide) has been investigated by Stor and coworkers.[14,21,26,27] We observe a CO dissociation process in **Mn$_2$CN$^+$** upon MLCT excitation.[22]

Table 1 Bond lengths of the two Mn–CO$_{axial}$ bonds, ^{13}C NMR shifts of the carbonyl carbons, and IR stretching frequencies of the axial CO ligands

	Bond length of Mn–C (Å)	^{13}C NMR (ppm)	IR stretch of CO (cm^{-1})
Mn–CO$_{axial}$ *trans* to C-terminus	1.840	220.4	2044
Mn–CO$_{axial}$ *trans* to N-terminus	1.817	220.1	2035

To understand the nature of the photo-induced intermediate, **s-Mn$_2$CN$^+$**, and the dynamics of the observed photochemistry, the photo-evolution of the intermediate was monitored *via in situ* IR spectroscopy during excitation of the MLCT transition using 395 nm light. Results of the IR photolysis are presented in Fig. 3 and the following observations are made: first, the higher frequency mode of the two axial CO stretches near 2050 cm^{-1} in **Mn$_2$CN$^+$** are absent post radiation. Second, an additional CO stretching mode appears near 1870 cm^{-1}. Last, the bridging-CN mode at ~2150 cm^{-1} decreases, while a new bridging cyanide peak grows in around 2120 cm^{-1}.

Although we have hypothesized the formation of **s-Mn$_2$CN$^+$** as a photochemical intermediate, it is also conceivable that there is loss of the axial CO *trans* to the N-terminus of the cyanide bridge to form an **Mn$_2$CN$^+$-s** intermediate rather than **s-Mn$_2$CN$^+$**. To explore this possibility and verify the identity of the intermediate, we performed vibrational analysis of the pristine **Mn$_2$CN$^+$** and the proposed MeCN-ligated intermediates (**Mn$_2$CN$^+$-s** and **s-Mn$_2$CN$^+$**). In Fig. 4, computed vibrational spectra are compared with the IR spectrum obtained after 60 s of irradiation at 395 nm (Fig. 3). After this reaction time, the MeCN-substituted intermediate is expected to be the majority species present. The simulated vibrational result based on the optimized geometry of **s-Mn$_2$CN$^+$** predicts two additional vibrational modes at 1870 cm^{-1} and 2125 cm^{-1}, which are attributed to carbonyls *trans* to bpy and bridged-CN stretching modes, respectively. These calculations predict that the main difference in vibrational spectra between **Mn$_2$CN$^+$-s** and **s-Mn$_2$CN$^+$** are the CO stretching modes between

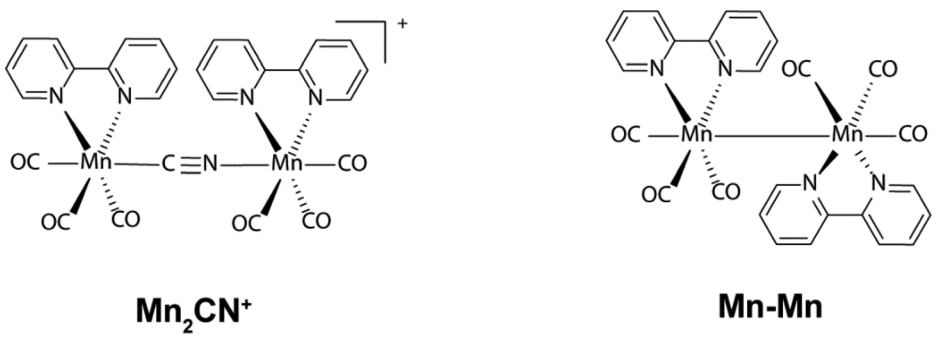

Fig. 1 Molecular representation of [{[Mn(bpy)(CO)$_3$]$_2$}(μ-CN)]$^+$ (**Mn$_2$CN$^+$**) and [(CO)$_3$(bpy)Mn–Mn(bpy)(CO)$_3$] (**Mn–Mn**).

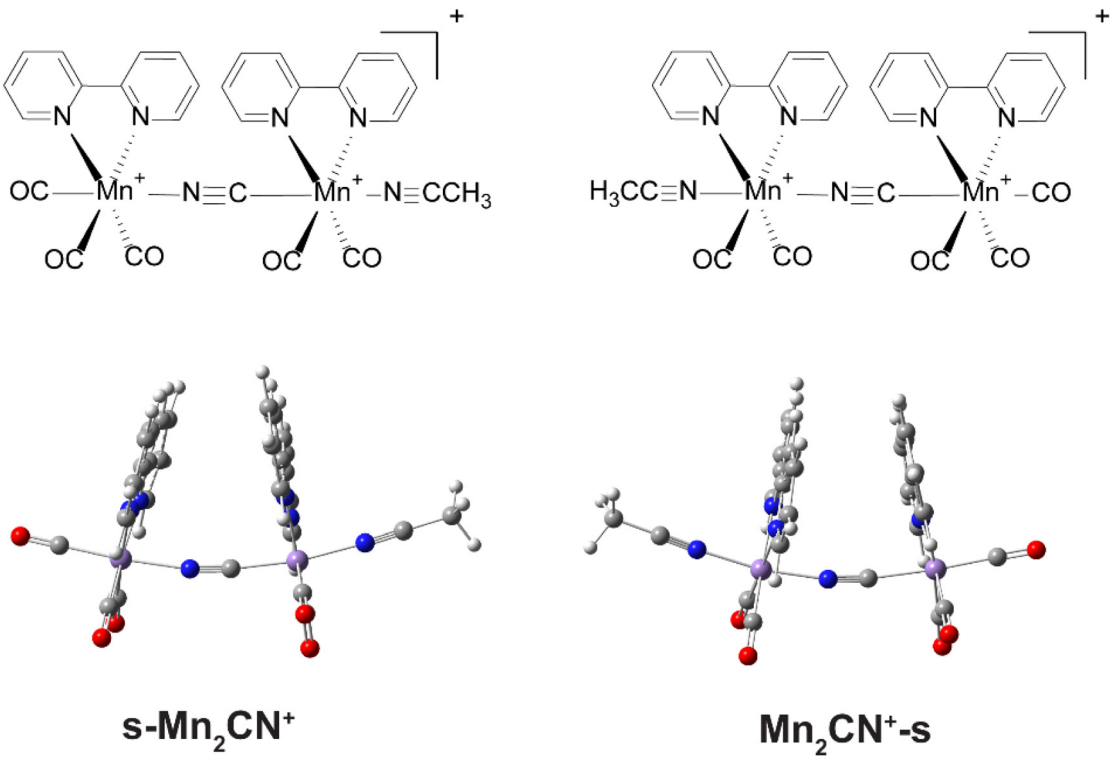

Fig. 2 Representations of the two proposed primary photoproducts derived from single crystal X-ray analysis,[22] showing potential sites for CO photosubstitution by the solvent, acetonitrile.

1850–1900 cm^{-1}. Specifically, **Mn_2CN^+-s** is expected to have a vibrational band near 1900 cm^{-1}. This predicted spectroscopic feature is significantly displaced compared to those observed in the experimental IR photolysis. On the other hand, the simulated vibrational line spectra of **s-Mn_2CN^+** nicely accounts for the changes observed in the IR spectra. We emphasize that the vibrational feature at 1880 cm^{-1} observed in the IR photo-

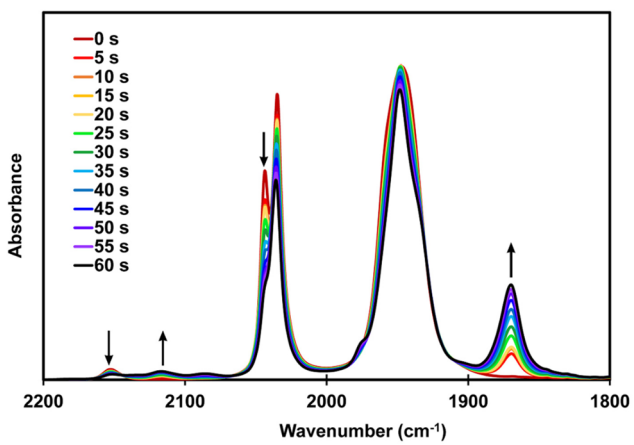

Fig. 3 IR spectra measured every 5 s from 0–60 s upon 395 nm photolysis of 10 mM **Mn_2CN^+** in degassed MeCN at 298 K.

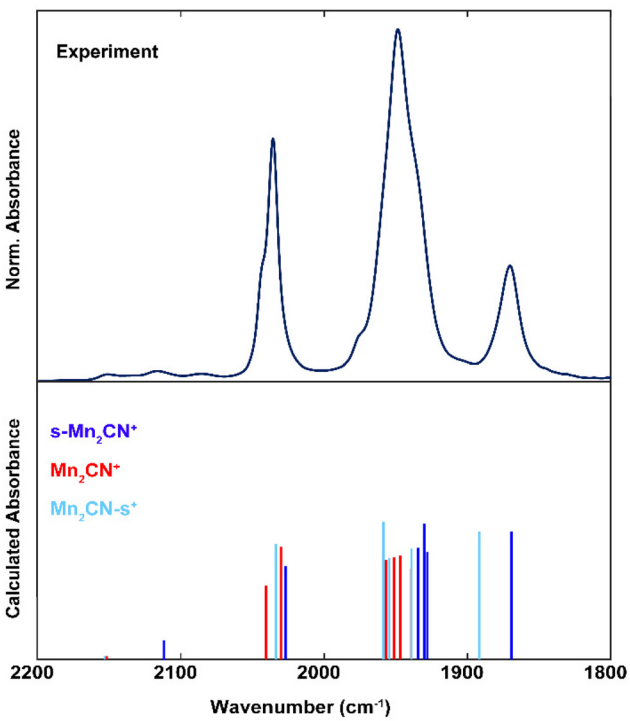

Fig. 4 Comparison of experimental data after 60 s photolysis from Fig. 3 and simulated spectra of the proposed intermediates **s-Mn_2CN^+** (dark blue), **Mn_2CN^+-s** (light blue) and the starting material, **Mn_2CN^+**.

lysis experiment is characteristic and exclusive to **s-Mn_2CN^+**. Hence, we rule out formation of **Mn_2CN^+-s**. To rule out other likely possibilities for this intermediate, we compared the IR spectrum to those of [Mn(bpy)$(CO)_3$CN] and [Mn(bpy)$(CO)_3$(MeCN)](PF_6) in Fig. S1.†

To further study the initial photophysics of **Mn_2CN^+**, transient absorption (TA) experiments were carried out in MeCN solvent (Fig. 5). Spectral evolution of a stirred solution of **Mn_2CN^+** in degassed MeCN is displayed in Fig. 5(a) and shows a broad photoinduced absorption (PIA) spanning from ~425 nm to 650 nm. This PIA appears immediately upon photoexcitation when the sample is stirred within the cuvette during the experiment. Over ~7 ns, the timespan of the experiment, there is little to no decay of this PIA.

However, when an air-free sample is not stirred during the experiment, several new negative signals arise, located at 460, 550, and 630 nm, as shown in Fig. 5(b). In the post-TA steady-state UV-vis spectrum, new peaks also arise at 461 and 633 nm. Stirring leads to the optically probed area of the sample being constantly replenished with complex that have not previously absorbed a photon. On the other hand, diffusional motion dominates when the sample is not stirred, allowing a greater amount of previously excited complex to remain in the probed sample volume, thereby allowing for the excitation of the primary photochemical products.

Following this logic, we hypothesize that two ground state products result from the decay of the **Mn_2CN^+** excited state: one immediately upon deactivation (which is the predominant species observed in the stirred experiment) and another through a bimolecular encounter process. When the sample is stirred, only the immediately formed species is observed due to continuous replenishment of the probed sample volume. Lack of agitation allows enough diffusively reacting species to accumulate in the probed region that the bimolecular product forms and appears in the TA spectrum. The bimolecular photoproduct peaks are located very near to the previously reported **Mn–Mn** dimer characteristic absorptions and, as such, are assigned to ground state bleaches (GSBs) of the **Mn–Mn** dimer.[14]

Additionally, when the TA experiment was performed in MeCN that was not rigorously air-free, the single, broad PIA signal persisted. The bimolecular photoproduct, the **Mn–Mn** dimer, was observed to be extremely air-sensitive and further, its formation is inhibited in the presence of O_2. However, the immediate photoproduct that is formed upon CO dissociation, **s-Mn_2CN^+**, is stable in the presence of O_2. Upon comparison of the UV-vis spectra measured before and after TA experiments, with and without oxygen, we conclude that the persistent, broad PIA present in both degassed and non-degassed samples is **s-Mn_2CN^+**.

In air, the UV-vis of the **Mn_2CN^+** complex after irradiation at 395 nm develops a peak around 500 nm with an isosbestic point at 420 nm as shown in Fig. 6 (bottom). This is indicative of a 1 : 1 conversion to the photoproduct **s-Mn_2CN^+** as observed in the IR during the early time points (Fig. 3). However, in rigorously degassed MeCN, **Mn_2CN^+** is converted rapidly to **Mn–Mn**, indicated by the peaks at 394, 461, 633, and 806 nm in Fig. 6 (top).[15] Upon exposure of an oxygen-free irradiated sample to oxygen, the peaks correlating to the dimer disappear, and the spectrum resembles that of **Mn_2CN^+** under irradiation in aerobic MeCN. Specifically, a shoulder around 520 nm appears, indicative of **s-Mn_2CN^+**.[22] These experiments show that the **Mn–Mn** dimer will not form when oxygen is present, and if **Mn–Mn** is first formed under argon, will rapidly become oxidized upon exposure to oxygen.

An earlier report from our lab focused only on the initial photophysics of **Mn_2CN^+** identifying the photoinduced loss of a CO ligand, and as such, did not report the formation of **Mn–Mn**.[22] To study the initial photophysics of **Mn_2CN^+**, we had previously used a light source eleven orders of magnitude less intense than the light source used in this current work.[28] We now report that beyond the initial formation of **s-Mn_2CN^+**

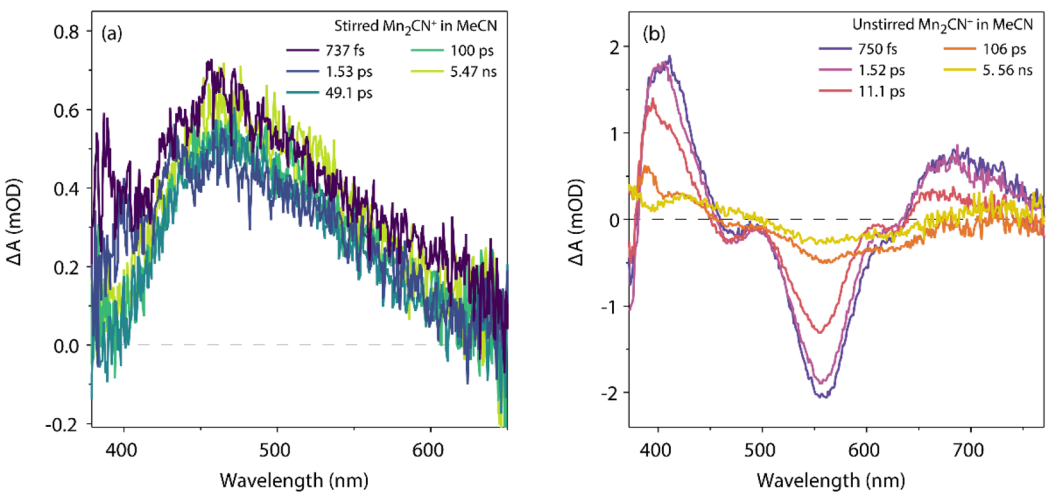

Fig. 5 Transient absorption spectra of **Mn_2CN^+** obtained (a) with stirring and (b) without stirring over the picosecond time regime (~0.74 to ~5500 ps) in degassed MeCN. Both samples were excited with a 365 nm pump.

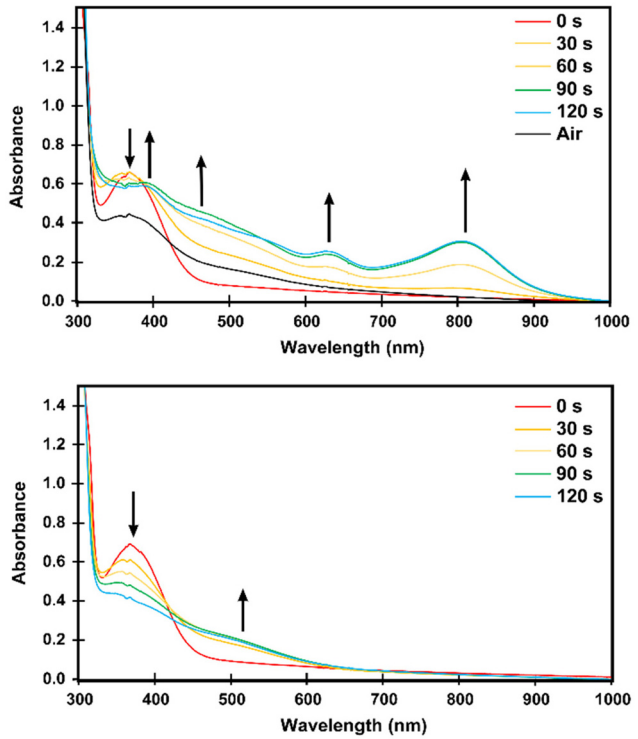

Fig. 6 UV-vis spectral changes of 0.1 mM $\mathbf{Mn_2CN^+}$ in degassed MeCN under Ar irradiated with a 395 nm LED (1 mW incident light) and then exposed to air after 120 s (top). UV-vis spectral changes during irradiation of 1 mM $\mathbf{Mn_2CN^+}$ in MeCN when open to the atmosphere (bottom).

observed by IR spectroscopy in the first minute of irradiation (Fig. 3), characteristic **Mn–Mn** dimer peaks arise at 1976, 1961, 1935, 1882, and 1856 cm^{-1} in the IR (Fig. 7).[14,19] These **Mn–Mn** dimer peaks only appear when the system is fully deoxygenated. The formation of **Mn–Mn** from $\mathbf{s\text{-}Mn_2CN^+}$ necessitates

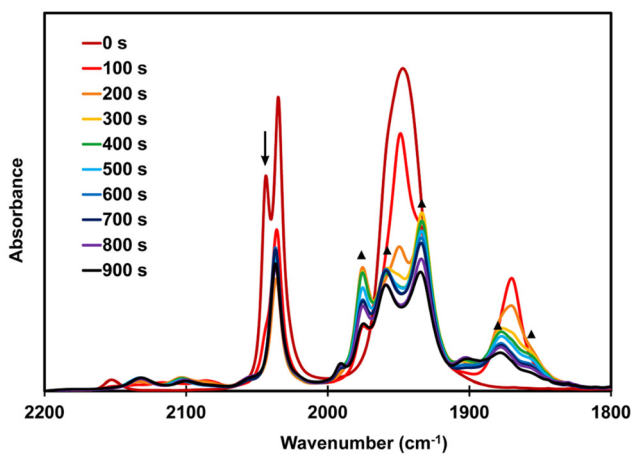

Fig. 7 Liquid phase IR spectra changes of 10 mM Mn_2CN^+ in degassed MeCN every 100 s of 395 nm irradiation. Peaks at 1976, 1961, 1935, 1882, and 1856 cm^{-1} are attributed to **Mn–Mn** formation and indicated by triangles.[14,19]

that the cyanide bridge breaks to initially yield the two Mn^I species shown in Fig. 8.

The peak at 2090 cm^{-1} in the IR in Fig. 7 is characteristic of a terminal cyanide peak and we attribute this to the $[Mn^I(bpy)(CO)_2(CN)(MeCN)]$ species. Terminal cyanide peaks tend to be located at lower wavenumbers than bridging cyanide peaks, and thus can be differentiated from each other.[22] The variation in ligand spheres about the two primary products will produce different Mn^0/Mn^I redox potentials for each. We hypothesize that disproportionation between these two Mn(I) species forms $[Mn(bpy)(CO)_3^{\bullet}]$ and $[Mn^{II}bpy(CO)_3(MeCN)]^+$. Coupling two $[Mn(bpy)(CO)_3^{\bullet}]$ fragments so formed is proposed to produce the **Mn–Mn** dimer along with $[Mn^{II}(bpy)(CO)_2(CN)(MeCN)]^+$ as outlined in Scheme 1.

To test this hypothesis, the EPR spectrum of 1 mM $\mathbf{Mn_2CN^+}$ in degassed MeCN was measured at 10 K before and after irradiation (395 nm) at room temperature. While the initial sample does not yield an EPR signal, one is observed after irradiation (Fig. 9). The spectrum features a broad signal centered at g_{iso} = 1.995 without hyperfine splitting. This signal is assigned to a low spin, d^5 Mn^{II} species based on literature reports for similar monomeric Mn^{II} complexes and the strong field nature of the carbonyl ligands.[29–32] Thus, the anticipated Mn^{II} product is observed.

As depicted in Scheme 1, the proposed reaction mechanism, involves two, one-photon processes to form **Mn–Mn** from $\mathbf{Mn_2CN^+}$. Since, the $[Mn^I(bpy)(CO)_2(CN)(MeCN)]$ intermediate acts as the electron donor and two of these are needed for every **Mn–Mn** dimer formed, this species is thought to be the limiting reagent in this reaction.

As previously reported, a requirement for CO_2 photoreduction using this class of Mn tricarbonyl complexes is the presence of a proton source, which is thought to stabilize the M–CO_2 adduct and facilitate cleavage of a C–O bond.[15,16] Photolysis studies were performed with concurrent UV-vis spectroscopy using 0.1 mM $\mathbf{Mn_2CN^+}$ in CO_2-saturated 5% v/v H_2O : MeCN. The time evolved UV-vis spectra measured over the course of the ten-minute photolysis experiment show **Mn–Mn** formation (Fig. 10).

The corresponding concentration of **Mn–Mn** and the total amount of CO produced over the course of this photolysis experiment is shown in Fig. 11. The concentration of **Mn–Mn** was determined using the reported extinction coefficient of 11 500 M^{-1} cm^{-1} at 805 nm.[33] After 120 s, the concentration of

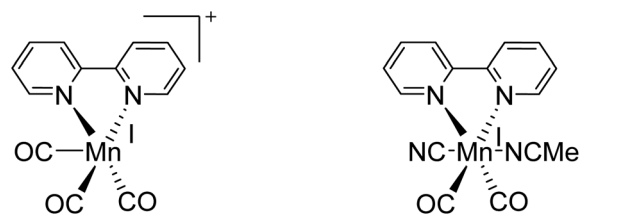

Fig. 8 A schematic of the two Mn^I species formed upon the breaking of the cyanide bridge.

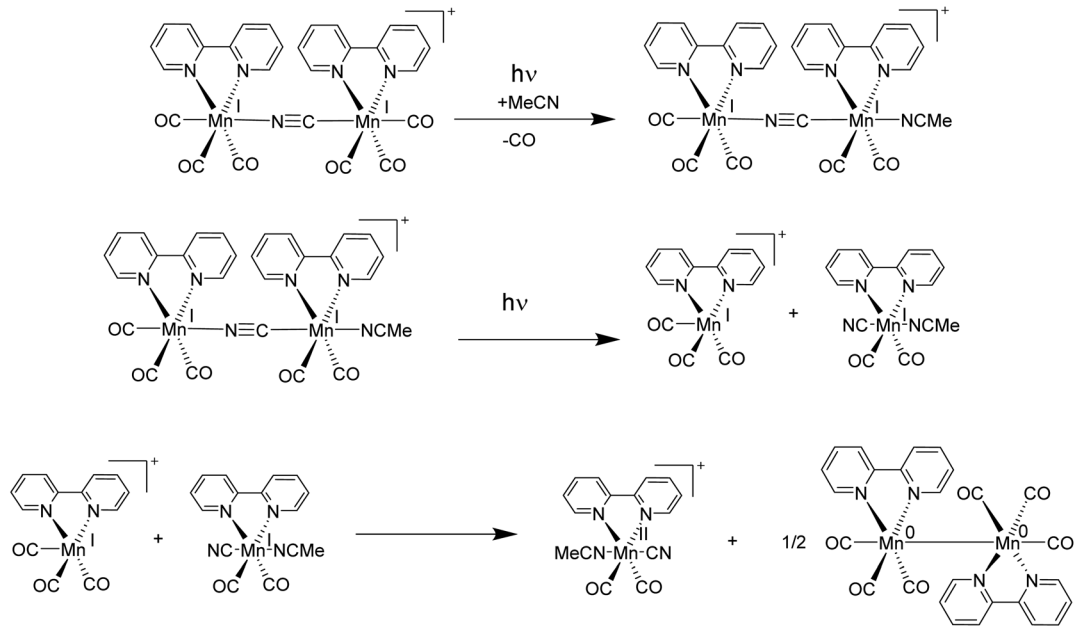

Scheme 1 Proposed reaction scheme for the formation of **Mn–Mn** from $\mathbf{Mn_2CN^+}$.

Mn–Mn reaches a maximum, corresponding to 21.2 micromolar **Mn–Mn**. The presence of **Mn–Mn** in solution corresponds with the production of CO, as shown in Fig. 11a.

To verify that $\mathbf{Mn_2CN^+}$ is capable of converting CO_2 to CO, $^{13}CO_2$ was employed in a control experiment using 1 M phenol as the proton source. It was found that $^{13}CO_2$ is not converted to ^{13}CO in the presence of oxygen. That is, in this case, the observed CO is ^{12}CO, which is derived from extensive ligand

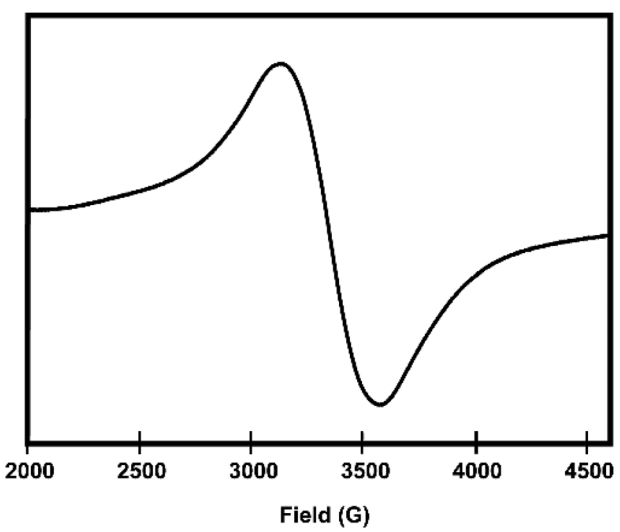

Fig. 9 X-band EPR spectrum (10 K) of 1 mM Mn_2CN^+ in degassed MeCN after room temperature irradiation at 395 nm for 10 min followed by immediately freezing at 4 K.

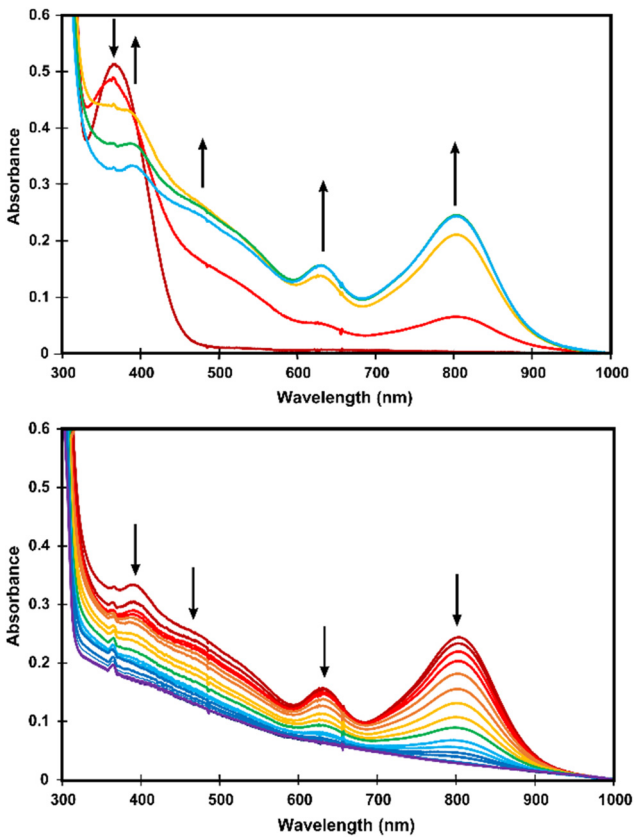

Fig. 10 UV-vis spectra of 0.1 mM $\mathbf{Mn_2CN^+}$ in CO_2-saturated MeCN taken every 30 s during 395 nm irradiation (2.97×10^{-9} einstein per s intensity), and showing an increase in dimer concentration from 0–120 s (top) and decrease in dimer formation (bottom) from 120–600 s.

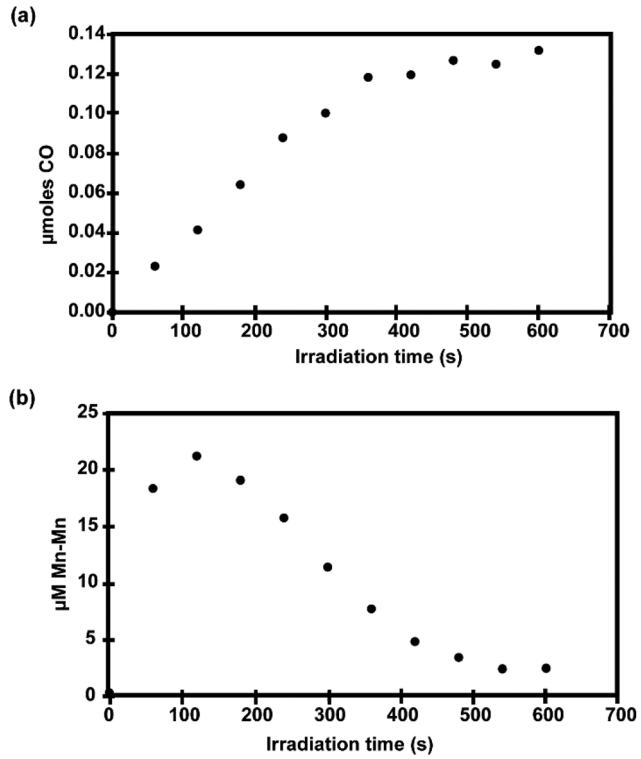

Fig. 11 (a) Carbon monoxide produced and (b) **Mn–Mn** formed during a photochemical CO_2 reduction experiment using 0.1 mM $\mathbf{Mn_2CN^+}$ in CO_2-saturated wet (5% v/v H_2O) MeCN under 395 nm light irradiation.

dissociation. It is only when the MeCN solvent is thoroughly degassed using the freeze–pump–thaw method that a ^{13}CO product is observed *via* gas phase IR (Fig. S2†), confirming the photochemical conversion of CO_2 to CO. A 3 mL sample of 1 mM $\mathbf{Mn_2CN^+}$ in $^{13}CO_2$-saturated MeCN, using 1 M phenol as the proton source, was irradiated for 30 min at 395 nm. The total quantum yield for CO was 0.64 with 5.0 micromoles of CO detected in the headspace. Using the ratio of $^{13}CO/^{12}CO$ found in the corresponding gas phase IR spectrum, the corrected quantum yield for the photoreduction of CO_2 to CO is 0.04. It is important to note that prior photochemical studies of manganese carbonyl complexes did not differentiate between dissociated CO and the CO produced from CO_2 reduction, when reporting quantum yields.[22,33] This has produced an improper picture of the efficiency at which the complexes of interest convert CO_2 to CO.

The role of the **Mn–Mn** dimer in electrochemical CO_2 reduction has been debated previously by various authors, including Ishitani,[34] Deronzier,[15,29] and Kubiak.[16] Kubiak hypothesized that the **Mn–Mn** bond would cleave homolytically first, as this behavior has been seen for similar **Mn–Mn** species,[35–37] before gaining another electron from an electron donor. Deronzier and coworkers note that the related $[Mn^0(dmbpy)(CO)_3]_2$ dimer[29] is capable of electrocatalytic CO_2 reduction. After generating $[Mn^0(dmbpy)(CO)_3]_2$ dimer electrochemically, it was reported that exposure to CO_2 led to an EPR signal correlated with a Mn^{II}-C(O)OH species. It was theorized to have formed after CO_2 and H^+ directly interacted *via* oxidative addition with $[Mn^0(dmbpy)(CO)_3]_2$.[29]

To further explore the chemistry of **Mn–Mn**, the dimer was directly synthesized by one of three methods, shown in Scheme 2. By using method A, the entire experiment can be kept in the dark, from synthesis to reaction with CO_2, allowing the evaluation of this complex with CO_2 under purely thermal conditions. In contrast, methods B and C provide two ways in which CO_2 can be introduced to the reaction vessel before **Mn–Mn** is formed.

The formation of **Mn–Mn** upon irradiation of $[Mn(bpy)(CO)_3Br]$ has been studied previously by Oskam *et al.*[14] The formation of **Mn–Mn** upon irradiation of $[Mn(bpy)(CO)_3(MeCN)]^+$ is presented here, and monitored by UV-vis and IR spectroscopies (Fig. S3†). First, $[Mn(bpy)(CO)_3(MeCN)]^+$ forms $[Mn(bpy)(CO)_2(MeCN)_2]^+$ after initial exposure to 395 nm light. In the dark, $[Mn(bpy)(CO)_3(MeCN)]^+$ and $[Mn(bpy)(CO)_2(MeCN)_2]^+$ do not react further with each other and are stable in solution even after 12 h as determined by UV-visible spectroscopy (Fig. 12). Irradiating a mixture of $[Mn(bpy)(CO)_3(MeCN)]^+$ and $[Mn(bpy)(CO)_2(MeCN)_2]^+$ at 517 nm, which is selectively absorbed by the dicarbonyl species, $[Mn(bpy)(CO)_2(MeCN)_2]^+$, also does not lead to **Mn–Mn** formation. However, irradiating the mixture with 395 nm light, which is absorbed by $[Mn(bpy)(CO)_3(MeCN)]^+$, leads to the formation of **Mn–Mn**. From this, we conclude that the dicarbonyl species, $[Mn(bpy)(CO)_2(MeCN)_2]^+$, donates an electron to the excited state of $[Mn(bpy)(CO)_3(MeCN)]^+$, forming $[Mn(bpy)(CO)_3(MeCN)]^0$ and $[Mn(bpy)(CO)_2(MeCN)_2]^{2+}$. The coupling together of two $[Mn(bpy)(CO)_3(MeCN)]^0$ moieties then leads to the formation of **Mn–Mn**, following Scheme 3.

The dominant species present in solution after the reaction of CO_2 with **Mn–Mn**, generated from methods A and B, was the reformation of the starting material. If **Mn–Mn** was generated from the irradiation of $[Mn(bpy)(CO)_3Br]$ or the chemical reduction of $[Mn(bpy)(CO)_3Br]$ using Na(Hg), then exposure to CO_2 led to the reformation of $[Mn(bpy)(CO)_3Br]$. Similarly, if **Mn–Mn** was formed *via* irradiation of $[Mn(bpy)(CO)_3(MeCN)]^+$, the primary product after the introduction of CO_2 was the reformation of $[Mn(bpy)(CO)_3(MeCN)]^+$ (Fig. S4 and S5†).

In addition to introducing CO_2 after **Mn–Mn** formation, CO_2 was also added to the monomeric precursors before irradiation using method B. When either $[Mn(bpy)(CO)_3Br]$ or $[Mn(bpy)(CO)_3(MeCN)]^+$ are irradiated in MeCN that is already saturated with CO_2, no **Mn–Mn** is observed (Fig. S6 and S7†). These results strongly imply that CO_2 is interacting with the radical precursor to **Mn–Mn**, suppressing dimer formation. A similar result was observed by Meyer for the rhenium analogue.[38]

It is well known that photolysis of metal–metal bonded dimers can lead to the homolytic cleavage of the metal–metal bond.[35,36,39] In cases where **Mn–Mn** is irradiated, it is expected that $\mathbf{Mn^{\bullet}}$ forms. However, we now report that even in the dark, **Mn–Mn** is thermally unstable at room temperature and will dissociate to form the radical species over the course of an hour under argon, as monitored *via* UV-vis spectroscopy

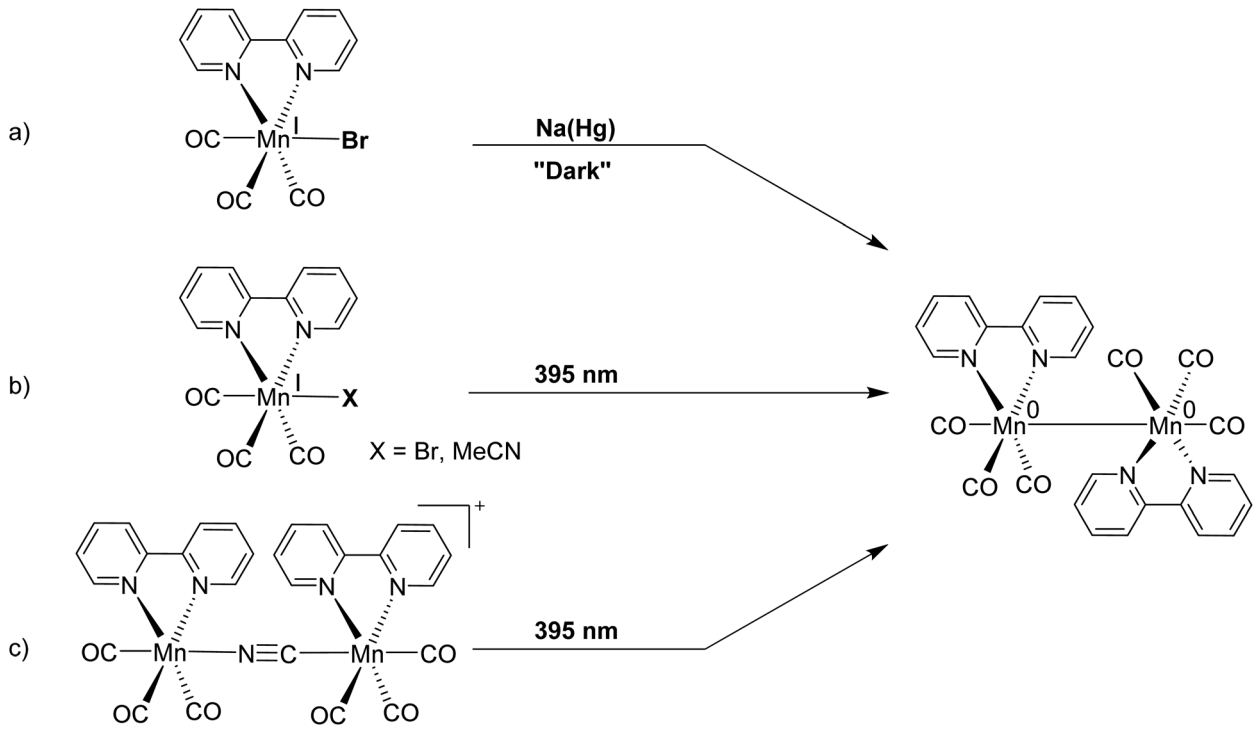

Scheme 2 Three methods for forming **Mn–Mn**.

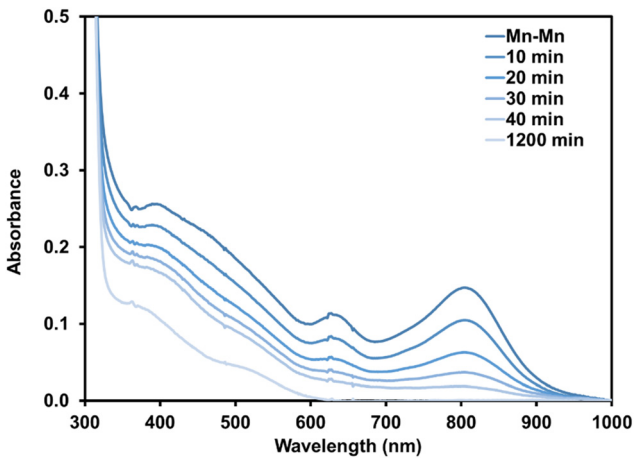

Fig. 12 UV-vis spectra of **Mn–Mn** synthesized from the initial irradiation of $[Mn(bpy)(CO)_3(MeCN)]^+$ in degassed MeCN, left in the dark under argon at room temperature. The two peaks at 375 nm and a shoulder ~500 nm correspond to $[Mn(bpy)(CO)_3(MeCN)]^+$ and $[Mn(bpy)(CO)_2(MeCN)_2]^+$, respectively.

(Fig. 12). Thus, even without irradiation, the **Mn$^\bullet$** species will be present in solution.

To evaluate the observed thermal instability of **Mn–Mn**, PPh_3 was introduced into a solution of **Mn–Mn** in the dark. The resultant solution was monitored by ^{31}P NMR, revealing the formation of a $[Mn(bpy)(CO)_3(PPh_3)]^+$ species. The same product was observed by ^{31}P NMR when a mixture of $[Mn(bpy)(CO)_3(MeCN)]^+$ and PPh_3 was irradiated with 395 nm light (Fig. S8†). The formation of a PPh_3-coordinated complex under these conditions shows that **Mn–Mn** does cleave in the dark to form $[Mn(bpy)(CO)_3^\bullet]$, and that its open coordination site can bind PPh_3. Similarly, we propose that $[Mn(bpy)(CO)_3^\bullet]$, thermally formed from **Mn–Mn** dissociation is capable of binding CO_2 in the dark.

To further demonstrate that light is not required to bind CO_2 with $[Mn(bpy)(CO)_3^\bullet]$, a solution of **Mn–Mn** was first synthesized in the dark from $[Mn(bpy)(CO)_3Br]$ and Na(Hg) following method A. This method insured that **Mn–Mn** could not have homolytically cleaved due to any light used to photochemically synthesize **Mn–Mn** from a monomeric precursor. A CO_2-saturated MeCN solution was then introduced in the dark to a degassed MeCN solution of **Mn–Mn** under argon. The reaction solution changed color from dark green-brown to orange upon addition of the CO_2 solution. While the solution under argon containing only **Mn–Mn** in degassed MeCN is EPR silent, a distinct Mn^{II} signal arose when CO_2 was added to the solution (Fig. S9†). This Mn^{II} signal is consistent with the theory that two electrons are donated by the Mn^0 center to reduce CO_2.[29,32] Attempts to further study this Mn^{II} species *via* UV-vis were unsuccessful. Although Deronzier suggested that the related *mer*-$[Mn^{II}(dmbpy)(CO)_3(C(O)OH)]^+$ species was stable due to persistent peaks in the UV-vis at λ_{max} = 360 and 500 nm,[29] these peaks most likely correspond to the solvent-ligated Mn complexes: $[Mn(dmbpy)(CO)_3(MeCN)]^+$ and $[Mn(dmbpy)(CO)_2(MeCN)_2]^+$. To explore this idea, the complexes, $[Mn(bpy)(CO)_3(MeCN)]^+$ and $[Mn(bpy)(CO)_2(MeCN)_2]^+$, were

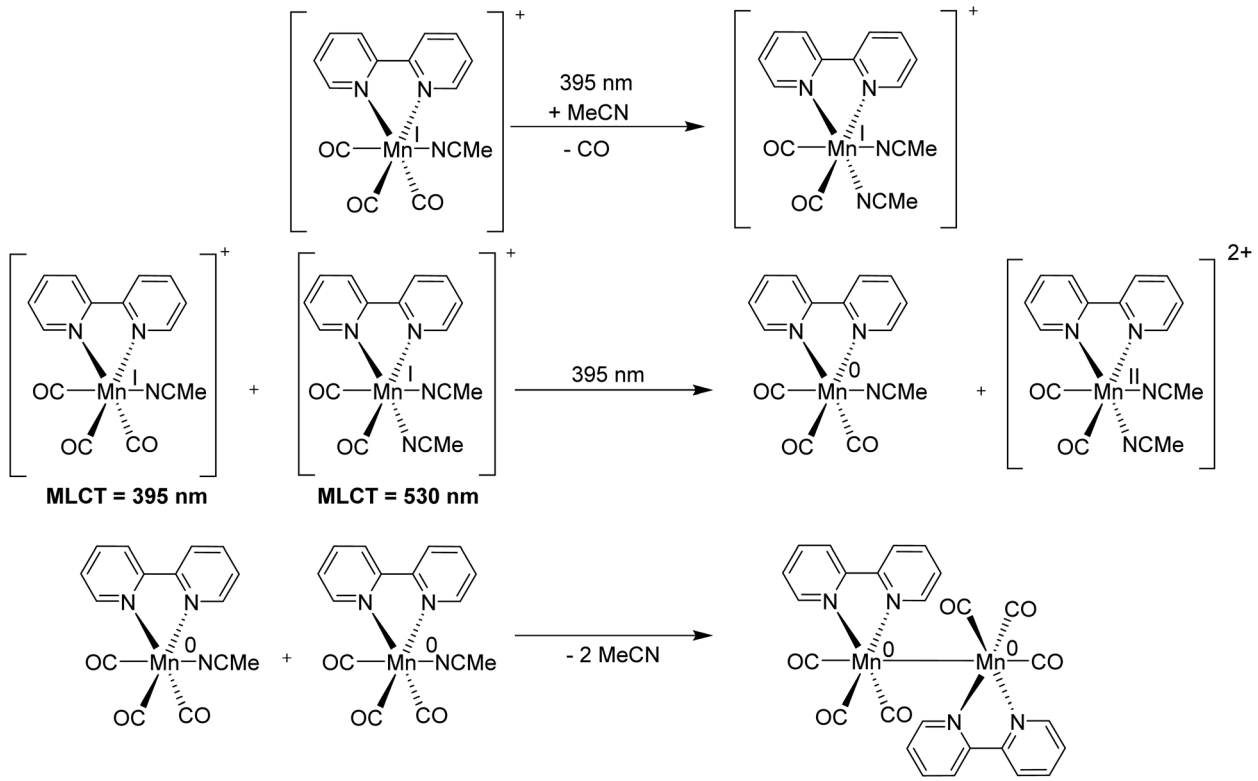

Scheme 3 Proposed mechanism for the photochemical synthesis of **Mn–Mn** from $[Mn(bpy)(CO)_3(MeCN)]^+$.

synthesized independently and their UV-vis spectra were found to match those two peaks, respectively. Thus, the prior literature and our IR spectroscopic analysis argue for the reaction depicted in Scheme 4.

In support of the reactivity shown in Scheme 4, the liquid phase IR spectrum that resulted from the dark reaction between **Mn–Mn** and CO_2 (Fig. 13) revealed a peak at 1633 cm^{-1} in the OCO stretching region, characteristic of a carboxylic acid group bound to a metal center.[40,41] This 1633 cm^{-1} does not correspond to known signals for free HCO_3^-/CO_3^{2-} which would be located at 1684 and 1646 cm^{-1},[42] or for water which would appear at 1654 cm^{-1}.[43] The peaks at 2027, 1933, and 1923 cm^{-1} correlate with $[Mn(bpy)(CO)_3Br]$, while the small shoulder peaks at 2049 and 1957 cm^{-1} are due to $[Mn(bpy)(CO)_3(MeCN)]^+$. When this solution, now mostly containing $[Mn(bpy)(CO)_3Br]$ is irradiated at 395 nm, **Mn–Mn** is regenerated, the peak at 1633 cm^{-1} increases slightly, and a small peak at 2036 cm^{-1} is more clearly revealed (Fig. S4†). The peak at 2036 cm^{-1} is identified as an axial carbonyl ligand based upon similar species, which is most likely associated with the Mn^{II}-C(O)OH intermediate shown in Scheme 4.[18,20] Although, this vibration is ~20 cm^{-1} higher than the reported axial carbonyl peaks for the *fac*-[Mn^{I}-C(O)OH] and *fac*-[Re^{I}-C(O)OH] species,[44,45] this shift in peak

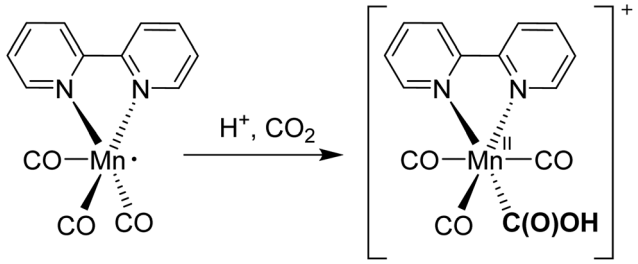

Scheme 4 Proposed mechanism of the dark reaction between $[Mn(bpy)(CO)_3^{\bullet}]$ and CO_2, resulting in a Mn^{II} complex.

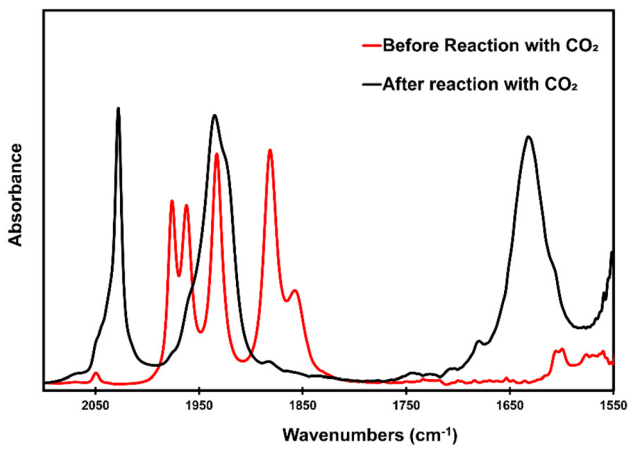

Fig. 13 IR spectra before and after **Mn–Mn** in degassed MeCN was quickly combined with CO_2-saturated MeCN in the dark.

position can be accounted for by the difference in their isomeric forms.[14]

While there is a dark reaction between [Mn(bpy)(CO)$_3^{\bullet}$] and CO_2, gas phase IR spectroscopy (Fig. S10†) shows that no CO is produced in the dark over the course of 1 h by this reaction. Only after irradiating a solution of **Mn–Mn**, in the presence of protons at 395 nm, is CO detected in the headspace gas. It is likely that this CO comes from the photochemical decomposition of **Mn–Mn**.

Conclusion

In conclusion, the photoevolution of the CN-bridged **Mn$_2$CN$^+$** in MeCN was examined using UV-vis and IR spectroscopy. Excitation of the MLCT state promotes axial CO dissociation followed by MeCN solvent ligation. By comparing experimental observables with computational results, we demonstrated that the identity of the intermediate is MeCN ligated at the C-terminus of the complex (**s-Mn$_2$CN$^+$**), rather than the N-terminus (**Mn$_2$CN$^+$-s**). Moreover, excited-state dynamics of **Mn$_2$CN$^+$** were investigated by TA spectroscopy with and without stirring of the reaction media. In the coordinating solvent (MeCN), there is a long-lived (~7 ns) PIA corresponding to **s-Mn$_2$CN$^+$** when the solution is stirred, with and without the presence of oxygen. Without stirring in degassed MeCN, ground state bleaches of the **Mn–Mn** dimer are observed.

We have also presented evidence for the unexpected role of trace O_2 in this chemistry as a destructive force that prevents **Mn–Mn** from forming. Since, **Mn–Mn** is relatively unstable at room temperature and dissociates in solution in the dark, we report that **Mn$^{\bullet}$** interacts with CO_2.

Photolysis experiments with concurrent UV-vis spectra show that the presence of **Mn–Mn** coincides with the generation of CO. This was further supported with gas phase IR evidence that $^{13}CO_2$ is only converted to ^{13}CO in the rigorous absence of O_2 and under irradiation. Previous literature accounts of Mn tricarbonyl complexes acting as CO production catalysts failed to take into account the CO formed by ligand dissociation. By using $^{13}CO_2$, true quantum yields for CO production *via* CO_2 reduction are reported here. Furthermore, we were able to show that a *mer* Mn^{II}-C(O)OH species is present after CO_2 is exposed to **Mn–Mn** through EPR and IR spectroscopies. Thus, we present a scheme for how **Mn–Mn** is generated from **Mn$_2$CN$^+$**, and suggest that the **Mn$^{\bullet}$** is the key photochemical reagent for CO_2 reduction to CO.

Experimental section

General

All reagents (reagent grade) were obtained from commercial suppliers and used without further purification unless otherwise noted. Anhydrous MeCN were purchased from Sigma-Aldrich (Sure/Seal) and degassed using the freeze–pump–thaw method before use. The {[Mn(bpy)(CO)$_3$]$_2$(μ-CN)}[ClO_4] (**Mn$_2$CN$^+$**) complex was synthesized according to the published method which couples [Mn(bpy)(CO)$_3$Br] to [Mn(bpy)(CO)$_3$CN] under an inert atmosphere using $AgClO_4$ in dry dichloromethane (DCM).[22] The complexes, [Mn(bpy)(CO)$_3$(MeCN)](PF_6) and [Mn(bpy)(CO)$_2$(MeCN)$_2$](PF_6), were synthesized following previous literature procedures.[15,46] **Mn–Mn** was synthesized from an adapted literature procedure where Na(Hg) was used instead of KC_8.[47] Samples were carefully handled with minimal light exposure.

Instrumentation

FT-IR spectra were recorded on a Nicolet Model iS50 FT-IR. The model of the optical filter used to follow photolysis experiments with simultaneous IR spectroscopy is Thorlabs NE2R05A. Ultrafast transient absorption measurements were conducted with pulses from a 1 kHz Ti:Sapphire regenerative amplifier system (Libra, Coherent). Libra produces ~45 fs 800 nm pulses at ~4 W power. Libra output was separated with a 90-10 (r-t) beam splitter to generate the pump and probe, respectively. The reflected portion of the beam was directed into a commercial optical parametric amplifier (OPerA, Coherent) to generate the 365 nm pump. Both the OPerA output and the transmitted portion of the of the 800 nm beam were directed into a commercial transient absorption spectrometer (Helios, Ultrafast system). The pump was chopped at 500 Hz. The transmitted 800 nm beam was mechanically delayed before being focused into a continuously translated CaF_2 window for white light generation. Relative pump and probe polarization was set at the "magic angle" using a π/2 waveplate in the path of the pump. Incident pump power was kept below 150 μW. UV–vis spectra were monitored using a Cary 60 UV–vis spectrophotometer (Agilent Technologies). EPR measurements at 10 K were performed on a Bruker EMXplus EPR Spectrometer outfitted with an Oxford liquid helium cryostat.

Photochemical and photophysical study

In the IR studies, the gastight, demountable liquid cell was assembled with two CaF_2 windows with 1 mm pathlength (PIKE, 162-1100-02). 10 mM **Mn$_2$CN$^+$** in MeCN was prepared and transferred to the IR cell in a glove box. To introduce CO_2 to **Mn–Mn**, a solution of **Mn–Mn** was rapidly mixed under inert atmosphere with CO_2-saturated MeCN and transferred to the IR cell immediately before data collection. In transient absorption studies, a solution of 300 μM analyte in MeCN was excited by a 365 nm laser and probed under constant stirring in a 2 mm path length quartz cuvette (Starna Cells) customized with a J Young joint. In the control experiment with $^{13}CO_2$, a solution of 5 mL degassed MeCN with 1 M phenol and 1 mM of **Mn$_2$CN$^+$** or 6 mM **Mn–Mn** in a clear borosilicate glass vial sealed with a PTFE/silicone septum (Supelco) was irradiated with a 395 nm LED light (3 W) under constant stirring and the headspace was sampled using a gas cell terminated by KBr plates. Photolysis experiments with $^{12}CO_2$ were carried out the same way and CO gas was detected *via* headspace analysis using a 120 °C isothermal method over 1.2 min on a HP 6890

Gas Chromatograph and TCD with a Molsieve 5A PLOT capillary column (Agilent) running He as the flow gas. UV-vis experiments were performed by loading a 1 cm pathlength quartz cuvette fitted with a septum with 0.1 mM Mn_2CN^+ in degassed MeCN in the glovebox. The cuvette was then tightly capped and for photolysis experiments, CO_2 was bubbled in for 15 min.

Computational methodology

Gaussian 16 [48] *via* density functional theory (DFT) with the M06 [49] functional level of theory and 6-311G** basis set[50] were used to perform geometry optimization and frequency calculations of the ground-state, singlet and doublet of molecules of interest. In order to alleviate computational cost, we applied LANL2DZ basis set on the manganese metal center. LANL2DZ basis set[51] describes inner electrons of the metal with effective core potentials. Additionally, polarizable continuum model (PCM)[52] with acetonitrile was utilized, since all photochemical measurements were conducted in the presence of acetonitrile. All frequency calculations carried out on stationary points yielded zero imaginary frequencies. HOMO and LUMO energy levels were extracted from the calculations.

Conflicts of interest

There are no conflicts to declare.

Acknowledgements

The authors acknowledge research funding from the National Science Foundation under grant no. CHE-1800400. G. D. S. gratefully acknowledges the Division of Chemical Sciences, Geosciences, and Biosciences, Office of Basic Energy Sciences of the US Department of Energy through grant no. DE-SC0015429. Dr John Eng is acknowledged for his help in measuring cryogenic EPR.

References

1 P. W. Huber and M. P. Mills, *The bottomless well: the twilight of fuel, the virtue of waste, and why we will never run out of energy*, Basic Books, 2007.
2 E. E. Benson, C. P. Kubiak, A. J. Sathrum and J. M. Smieja, Electrocatalytic and homogeneous approaches to conversion of CO 2 to liquid fuels, *Chem. Soc. Rev.*, 2009, **38**(1), 89–99.
3 A. M. Appel, J. E. Bercaw, A. B. Bocarsly, H. Dobbek, D. L. DuBois, M. Dupuis, J. G. Ferry, E. Fujita, R. Hille and P. J. Kenis, Frontiers, opportunities, and challenges in biochemical and chemical catalysis of CO2 fixation, *Chem. Rev.*, 2013, **113**(8), 6621–6658.
4 J. L. White, M. F. Baruch, J. E. Pander, Y. Hu, I. C. Fortmeyer, J. E. Park, T. Zhang, K. Liao, J. Gu, Y. Yan, T. W. Shaw, E. Abelev and A. B. Bocarsly, Light-Driven Heterogeneous Reduction of Carbon Dioxide: Photocatalysts and Photoelectrodes, *Chem. Rev.*, 2015, **115**(23), 12888–12935.
5 J. M. Smieja and C. P. Kubiak, Re(bipy-tBu)(CO) 3Cl—improved Catalytic Activity for Reduction of Carbon Dioxide: IR-Spectroelectrochemical and Mechanistic Studies, *Inorg. Chem.*, 2010, **49**(20), 9283–9289.
6 J. Hawecker, J.-M. Lehn and R. Ziessel, Efficient photochemical reduction of CO_2 to CO by visible light irradiation of systems containing $Re(bipy)(CO)_3X$ or $Ru(bipy)_3^{2+}$–Co^{2+} combinations as homogeneous catalysts, *J. Chem. Soc., Chem. Commun.*, 1983, (9), 536–538.
7 J. Hawecker, J.-M. Lehn and R. Ziessel, Photochemical and Electrochemical Reduction of Carbon Dioxide to Carbon Monoxide Mediated by (2,2′-Bipyridine)tricarbonylchlororhenium(I) and Related Complexes as Homogeneous Catalysts, *Helv. Chim. Acta*, 1986, **69**(8), 1990–2012.
8 R. Francke, B. Schille and M. Roemelt, Homogeneously catalyzed electroreduction of carbon dioxide—methods, mechanisms, and catalysts, *Chem. Rev.*, 2018, **118**(9), 4631–4701.
9 D. C. Grills, M. Z. Ertem, M. Mckinnon, K. T. Ngo and J. Rochford, Mechanistic aspects of CO2 reduction catalysis with manganese-based molecular catalysts, *Coord. Chem. Rev.*, 2018, **374**, 173–217.
10 S. Kaneco, H. Katsumata, T. Suzuki and K. Ohta, Photoelectrochemical reduction of carbon dioxide at p-type gallium arsenide and p-type indium phosphide electrodes in methanol, *Chem. Eng. J.*, 2006, **116**(3), 227–231.
11 B. Jo'm and J. Wass, On the photoelectrocatalytic reduction of carbon dioxide, *Mater. Chem. Phys.*, 1989, **22**(3–4), 249–280.
12 M. Wrighton and D. L. Morse, Nature of the lowest excited state in tricarbonylchloro-1, 10-phenanthrolinerhenium(I) and related complexes, *J. Am. Chem. Soc.*, 1974, **96**(4), 998–1003.
13 S. Sato, Y. Matubara, K. Koike, M. Falkenström, T. Katayama, Y. Ishibashi, H. Miyasaka, S. Taniguchi, H. Chosrowjan and N. Mataga, Photochemistry of fac-[Re(bpy)(CO) 3Cl], *Chemistry*, 2012, **18**(49), 15722.
14 G. J. Stor, S. L. Morrison, D. J. Stufkens and A. Oskam, The Remarkable Photochemistry of fac-XMn(CO)3(.alpha.-diimine) (X = Halide): Formation of Mn2(CO)6(.alpha.-diimine)2 via the mer Isomer and Photocatalytic Substitution of X- in the Presence of PR3, *Organometallics*, 1994, **13**(7), 2641–2650.
15 M. Bourrez, F. Molton, S. Chardon-Noblat and A. Deronzier, [Mn(bipyridyl)$(CO)_3$Br]: An Abundant Metal Carbonyl Complex as Efficient Electrocatalyst for CO_2 Reduction, *Angew. Chem., Int. Ed.*, 2011, **50**(42), 9903–9906.
16 J. M. Smieja, M. D. Sampson, K. A. Grice, E. E. Benson, J. D. Froehlich and C. P. Kubiak, Manganese as a Substitute for Rhenium in CO_2 Reduction Catalysts: The Importance of Acids, *Inorg. Chem.*, 2013, **52**(5), 2484–2491.
17 M. D. Sampson and C. P. Kubiak, Manganese Electrocatalysts with Bulky Bipyridine Ligands: Utilizing

Lewis Acids To Promote Carbon Dioxide Reduction at Low Overpotentials, *J. Am. Chem. Soc.*, 2016, **138**(4), 1386–1393.

18 H.-Y. Kuo, S. E. Tignor, T. S. Lee, D. Ni, J. E. Park, G. D. Scholes and A. B. Bocarsly, Reduction-induced CO dissociation by a $[Mn(bpy)(CO)_4][SbF_6]$ complex and its relevance in electrocatalytic CO_2 reduction, *Dalton Trans.*, 2020, **49**(3), 891–900.

19 F. Hartl, B. D. Rossenaar, G. J. Stor and D. J. Stufkens, Role of an electron–transfer chain reaction in the unusual photochemical formation of five–coordinated anions $[Mn(CO)_3(\alpha\text{-diimine})]^-$ from fac-$[Mn(X)(CO)_3(\alpha\text{–diimine})]$(X = halide) at low temperatures, *Recl. Trav. Chim. Pays-Bas*, 1995, **114**(11–12), 565–570.

20 P. L. Cheung, C. W. Machan, A. Y. S. Malkhasian, J. Agarwal and C. P. Kubiak, Photocatalytic Reduction of Carbon Dioxide to CO and HCO_2H Using fac-$Mn(CN)(bpy)(CO)_3$, *Inorg. Chem.*, 2016, **55**(6), 3192–3198.

21 G. Stor, D. Stufkens, P. Vernooijs, E. Baerends, J. Fraanje and K. Goubitz, X-ray Structure of fac-$IMn(CO)_3$(bpy) and Electronic Structures and Transitions of the Complexes fac-$XMn(CO)_3$(bpy) (X = Cl, I) and mer-$ClMn(CO)_3$(bpy), *Inorg. Chem.*, 1995, **34**(6), 1588–1594.

22 H.-Y. Kuo, S. T. Lee, A. T. Chu, S. E. Tignor, G. D. Scholes and A. B. Bocarsly, A cyanide-bridged di-manganese carbonyl complex that photochemically reduces CO_2 to CO, *Dalton Trans.*, 2019, **48**(4), 1226–1236.

23 J. Jimenez, I. Chakraborty and P. K. Mascharak, Synthesis and assessment of CO-release capacity of manganese carbonyl complexes derived from rigid α-diimine ligands of varied complexity, *Eur. J.Inorg. Chem.*, 2015, **2015**(30), 5021.

24 V. Yempally, S. J. Kyran, R. K. Raju, W. Y. Fan, E. N. Brothers, D. J. Darensbourg and A. A. Bengali, Thermal and Photochemical Reactivity of Manganese Tricarbonyl and Tetracarbonyl Complexes with a Bulky Diazabutadiene Ligand, *Inorg. Chem.*, 2014, **53**(8), 4081–4088.

25 S. J. Carrington, I. Chakraborty and P. K. Mascharak, Rapid CO release from a Mn(I) carbonyl complex derived from azopyridine upon exposure to visible light and its phototoxicity toward malignant cells, *Chem. Commun.*, 2013, **49**(96), 11254–11256.

26 A. Rosa, G. Ricciardi, E. J. Baerends and D. J. Stufkens, Metal-to-Ligand Charge Transfer Photochemistry: Homolysis of the Mn−Cl Bond in the mer-$Mn(Cl)(CO)_3(\alpha\text{-diimine})$ Complex and Its Absence in the fac-Isomer, *Inorg. Chem.*, 1998, **37**(24), 6244–6254.

27 A. Rosa, G. Ricciardi, E. J. Baerends and D. J. Stufkens, Metal-to-ligand charge transfer (MLCT) photochemistry of fac-$Mn(Cl)(CO)_3$(H-DAB): a density functional study, *J. Phys. Chem.*, 1996, **100**(38), 15346–15357.

28 In our previous paper, we used a different light source than we do in this manuscript. The intensity of the 365 nm laser used in the previous paper was 4×10^{-20} Einsteins per s and the intensity of the 395 nm LED used in this manuscript is 4.3×10^{-9} Einsteins per s. In 60 seconds, the 395 nm LED used in this manuscript delivers 2.6×10^{-7} Einsteins, which is nine orders of magnitude more than the 365 nm laser does in 60 minutes (1.6×10^{-16} Einsteins).

29 M. Bourrez, M. Orio, F. Molton, H. Vezin, C. Duboc, A. Deronzier and S. Chardon-Noblat, Pulsed-EPR Evidence of a Manganese(II) Hydroxycarbonyl Intermediate in the Electrocatalytic Reduction of Carbon Dioxide by a Manganese Bipyridyl Derivative, *Angew. Chem., Int. Ed.*, 2014, **53**(1), 240–243.

30 A. Popa, O. Raita, M. Stan, O. Pana, G. Borodi and L. Giurgiu, Electron paramagnetic resonance of Mn-doped $Sn_{1-x}Mn_xO_2$ powders, *Appl. Magn. Reson.*, 2012, **42**(4), 453–462.

31 A. T. Radosevich, J. G. Melnick, S. A. Stoian, D. Bacciu, C.-H. Chen, B. M. Foxman, O. V. Ozerov and D. G. Nocera, Ligand reactivity in diarylamido/bis(phosphine) PNP complexes of $Mn(CO)_3$ and $Re(CO)_3$, *Inorg. Chem.*, 2009, **48**(19), 9214–9221.

32 K. K. Singh, M. A. Siegler and V. S. Thoi, Unusual Reactivity of a Thiazole-Based Mn Tricarbonyl Complex for CO_2 Activation, *Organometallics*, 2020, **39**(7), 988–994.

33 H. Takeda, H. Kamiyama, K. Okamoto, M. Irimajiri, T. Mizutani, K. Koike, A. Sekine and O. Ishitani, Highly Efficient and Robust Photocatalytic Systems for CO_2 Reduction Consisting of a Cu(I) Photosensitizer and Mn(I) Catalysts, *J. Am. Chem. Soc.*, 2018, **140**(49), 17241–17254.

34 H. Takeda, H. Koizumi, K. Okamoto and O. Ishitani, Photocatalytic CO_2 reduction using a Mn complex as a catalyst, *Chem. Commun.*, 2014, **50**(12), 1491–1493.

35 M. S. Wrighton and D. S. Ginley, Photochemistry of metal-metal bonded complexes. II. Photochemistry of rhenium and manganese carbonyl complexes containing a metal-metal bond, *J. Am. Chem. Soc.*, 1975, **97**(8), 2065–2072.

36 D. L. Morse and M. S. Wrighton, Photochemistry of metal-metal bonded complexes. 5. Cleavage of the MM bond in $(OC)_5M$-M $(CO)_3L$ by irradiation into a low-lying M. fwdarw. L charge-transfer band, *J. Am. Chem. Soc.*, 1976, **98**(13), 3931–3934.

37 M. S. Wrighton and D. S. Ginley, Photochemistry of metal-metal bonded complexes. III. Photoreactivity of hexacarbonylbis (.eta. ^{5}-cyclopentadienyl) dimolybdenum(I) and-ditungsten(I), *J. Am. Chem. Soc.*, 1975, **97**(15), 4246–4251.

38 B. P. Sullivan, C. M. Bolinger, D. Conrad, W. J. Vining and T. J. Meyer, One- and two-electron pathways in the electrocatalytic reduction of CO2 by fac-Re(bpy)(CO)3Cl (bpy = 2,2′-bipyridine). Journal of the Chemical Society, *Chem. Commun.*, 1985, (20), 1414–1416.

39 T. J. Meyer and J. V. Caspar, Photochemistry of metal-metal bonds, *Chem. Rev.*, 1985, **85**(3), 187–218.

40 P. K. Chan and W. K. Leong, Reaction of Cp*Ir(CO)2 with Activated Perfluoroaromatic Compounds: Formation of Metallocarboxylic Acids via Aromatic Nucleophilic Substitution, *Organometallics*, 2008, **27**(6), 1247–1253.

41 D. H. Gibson, Y. Ding, J. G. Andino, M. S. Mashuta and J. F. Richardson, Synthesis, Characterization, and Reactions of Ruthenium Phenanthroline Complexes Bearing C1 Ligands: Formyl, Metallocarboxylate, and CO_2-

Bridged Complexes, *Organometallics*, 1998, **17**(23), 5178–5183.

42 F. Franco, C. Cometto, L. Nencini, C. Barolo, F. Sordello, C. Minero, J. Fiedler, M. Robert, R. Gobetto and C. Nervi, Local Proton Source in Electrocatalytic CO_2 Reduction with [Mn(bpy-R)$(CO)_3$Br] Complexes, *Chem. – Eur. J.*, 2017, **23**(20), 4782–4793.

43 C. W. Machan, C. J. Stanton, J. E. Vandezande, G. F. Majetich, H. F. Schaefer, C. P. Kubiak and J. Agarwal, Electrocatalytic Reduction of Carbon Dioxide by Mn(CN)(2,2′-bipyridine)$(CO)_3$: CN Coordination Alters Mechanism, *Inorg. Chem.*, 2015, **54**(17), 8849–8856.

44 M. R. Madsen, M. H. Rønne, M. Heuschen, D. Golo, M. S. G. Ahlquist, T. Skrydstrup, S. U. Pedersen and K. Daasbjerg, Promoting Selective Generation of Formic Acid from CO2 Using Mn(bpy)(CO)3Br as Electrocatalyst and Triethylamine/Isopropanol as Additives, *J. Am. Chem. Soc.*, 2021, **143**(48), 20491–20500.

45 M. D. Sampson, J. D. Froehlich, J. M. Smieja, E. E. Benson, I. D. Sharp and C. P. Kubiak, Direct observation of the reduction of carbon dioxide by rhenium bipyridine catalysts, *Energy Environ. Sci.*, 2013, **6**(12), 3748–3755.

46 V. Yempally, S. Moncho, F. Hasanayn, W. Y. Fan, E. N. Brothers and A. A. Bengali, Ancillary Ligand Effects upon the Photochemistry of Mn(bpy)$(CO)_3$X Complexes (X = Br^-, $PhCC^-$), *Inorg. Chem.*, 2017, **56**(18), 11244–11253.

47 C. W. Machan, M. D. Sampson, S. A. Chabolla, T. Dang and C. P. Kubiak, Developing a Mechanistic Understanding of Molecular Electrocatalysts for CO2 Reduction using Infrared Spectroelectrochemistry, *Organometallics*, 2014, **33**(18), 4550–4559.

48 M. Frisch, G. Trucks, H. Schlegel, G. Scuseria, M. Robb, J. Cheeseman, G. Scalmani, V. Barone, G. Petersson and H. Nakatsuji, *Gaussian 16*, Gaussian, Inc., Wallingford, CT, 2016.

49 Y. Zhao and D. G. Truhlar, The M06 suite of density functionals for main group thermochemistry, thermochemical kinetics, noncovalent interactions, excited states, and transition elements: two new functionals and systematic testing of four M06-class functionals and 12 other functionals, *Theor. Chem. Acc.*, 2008, **120**(1), 215–241.

50 K. U. D. Calvinho, A. B. Laursen, K. M. K. Yap, T. A. Goetjen, S. Hwang, N. Murali, B. Mejia-Sosa, A. Lubarski, K. M. Teeluck, E. S. Hall, E. Garfunkel, M. Greenblatt and G. C. Dismukes, Selective CO_2 reduction to C3 and C4 oxyhydrocarbons on nickel phosphides at overpotentials as low as 10 mV, *Energy Environ. Sci.*, 2018, **11**(9), 2550–2559.

51 T. H. Dunning Jr., Gaussian Basis Functions for Use in Molecular Calculations. I. Contraction of (9s5p) Atomic Basis Sets for the First–Row Atoms, *J. Chem. Phys.*, 1970, **53**(7), 2823–2833.

52 J. C. Slater and J. C. Phillips, Quantum Theory of Molecules and Solids Vol. 4: The Self–Consistent Field for Molecules and Solids, *Phys. Today*, 1974, **27**(12), 49–50.